Tectonophysics 765 (2019) 1–10

Contents lists available at ScienceDirect

Tectonophysics

journal homepage: www.elsevier.com/locate/tecto

Observed stress state for the IODP Site C0002 and implication to the stress field of the Nankai Trough subduction zone

Hung-Yu Wu[a,*], Chung-Han Chan[b], Kazuya Shiraishi[a], Adam Wspanialy[a], Takamitsu Sugihara[a], Yoshinori Sanada[a]

[a] Japan Agency for Marine-Earth Science and Technology, Japan
[b] Earth Observatory of Singapore, Nanyang Technological University, Singapore

ARTICLE INFO

Keywords:
Nankai Trough
Stress state
geomechanical model
Breakout
Optimally oriented plane modeling

ABSTRACT

Conducting a stress state analysis is one of major challenges for evaluating earth crust and formation conditions. Stress magnitude is especially essential to comprehend stress heterogeneity, significant structural anisotropy, and/or pre-existing fracture systems. Stress state is influenced by rock strength, structural properties, and near-field principal stresses, which impact borehole integrity during drilling. Factors that we can measure through Logging While Drilling (LWD) and Measure while Drilling (MWD) to better understand borehole conditions, include mud weight, overburden weight and velocity. The LWD resistivity images in Holes C0002A and C0002F of the Nankai Trough Seismogenic Zone Experiment (NanTroSEIZE) indicate that most of the drillings in stable environments. However, the bottom hole assembly became stuck around 3 km depth in Hole C0002P and did not reach the mega-thrust fault. We evaluated the stress state for the Site C0002 by the geomechanical model. With the breakout width and rock strength estimation, we constrain the stress profiles in the drilled depth. Our analysis inferred that the instability of Hole C0002P had been caused by an overpressure drilling fluid state and low horizontal principal stress. Furthermore, we developed an optimally oriented plane (OOP) model to exam the stress state in the Site C0002 from Nankai accretionary prism to the Nankai Trough subduction zone. The normal faulting stress regime modeled from OOP is consistent with the geomechanical model in Site C0002. The horizontal principal stresses magnitude appears to less than the overburden weight above this subduction zone.

1. Introduction

The Nankai Trough is created by the subduction of the Philippine Sea plate underneath the Eurasian plate at a drifting rate of ~4.1–6.5 cm/year (Seno et al., 1993). For better understanding its behavior, beginning in September 2007, the NanTroSEIZE (Nankai Trough Seismogenic Zone Experiment) executed multi-years, multi-stages drilling missions organized by the Integrated Ocean Drilling Program (IODP). Site C0002 is located in the Kumano forearc basin off the Kii Peninsula, Japan (Kinoshita et al., 2008). To study and evaluate the stress state in this regime (shown in Fig. 1a), Site C0002 is designed to be the primary site for drilling through fault zones. The primary objective of the drilling at Site C0002 is to investigate the mega-spray fault and interface of the plate boundary of the Nankai Trough (Kinoshita et al., 2008) using riserless/riser drilling (Fig. 1a). The subduction zone is expected at the depth of 7000 mbsf (meters below sea floor). Comprehensive LWD and MWD were collected from Holes C0002A, C0002F and Hole C0002P (Expedition 348 Scientists and Scientific Participants, 2014). These three stages of scientific drillings provide comprehensive logging data and drilling information to estimate the stress state and borehole conditions. LWD and Annular Pressure While Drilling (APWD) were deployed during different stages of these expeditions. During the drilling operations, swelling around the borehole and sticking pipes, which damaged the blowout preventer (BOP) in Hole C0002F (Moore et al., 2013), stopped the drilling at the depth of 2000 mbsf at Site C0002. The Japanese scientific drilling vessel Chikyu carried out alternative plans in an attempt to reach the target depth by drilling Holes C0002G-C0002P, as we presented in Fig. 1b. The drilling processes were stopped because of poor borehole conditions at the depth of 3058 mbsf in Hole C0002P (Expedition 348 Scientists and Scientific Participants, 2014). Comparing the LWD images in Holes C0002A, C0002F and C0002P, different borehole behaviors were observed in these three closely located boreholes. Borehole breakout was rarely seen in Holes C0002F and C0002P, which are the drillings that stop in the accretionary prism due to the drilling difficulties (such as pipe stuck, lost mud circulation). Borehole

* Corresponding author.
E-mail address: sonata@eqkc.earth.ncu.edu.tw (H.-Y. Wu).

https://doi.org/10.1016/j.tecto.2019.04.017
Received 20 August 2018; Received in revised form 10 April 2019; Accepted 14 April 2019
Available online 09 May 2019
0040-1951/

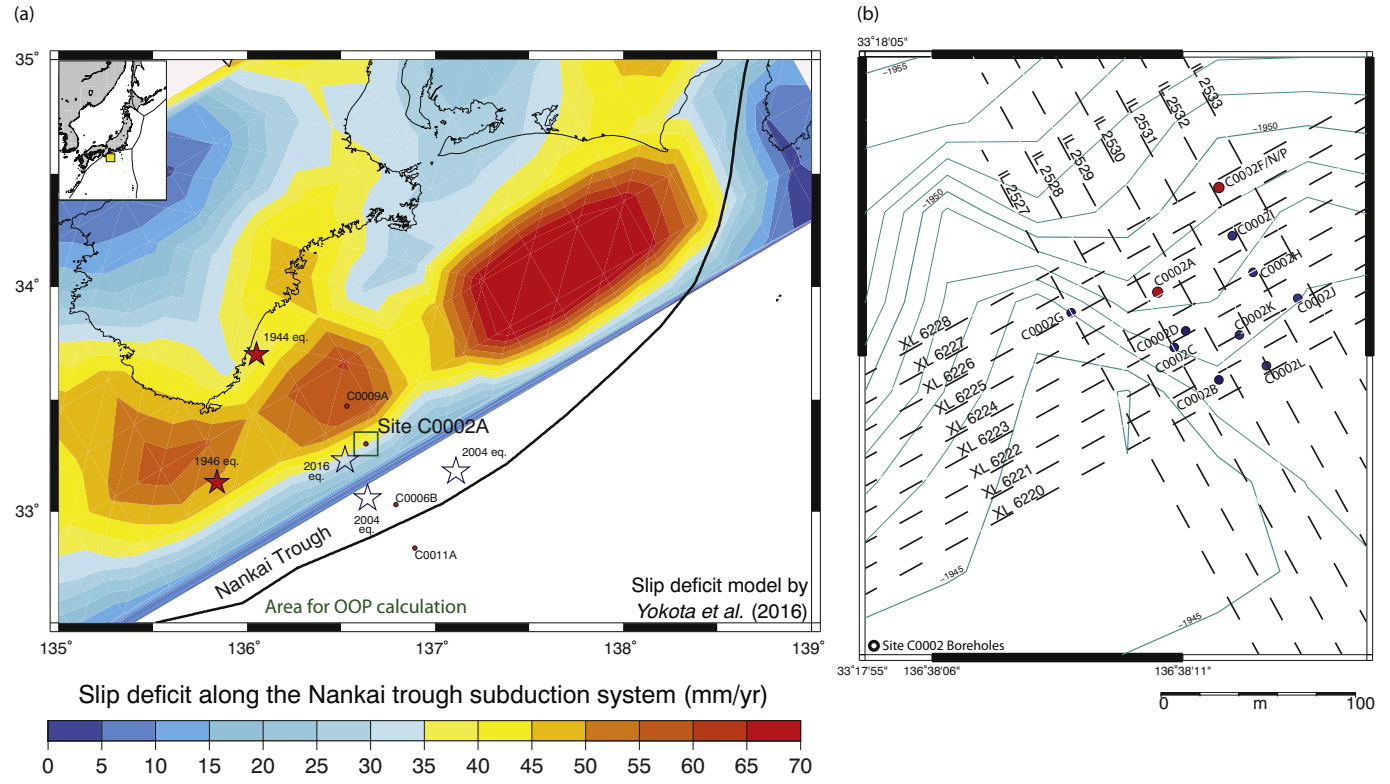

Fig. 1. (a) The slip deficit model in Nankai based on the observed data from Yokota et al. (2016). The square shows the main research area, Site C0002. The stars show the significant historical earthquakes. (b) Site map of Site C0002 serial boreholes drilled in expedition 314, 338, and 348. The cycles present the borehole location. The main investigated boreholes in this study are in red; the coring/observatory wells are marked in blue cycles. The black lines are the seismic profile, including the in-lines (IL) and cross-lines (XL). Green lines indicated the bathymetry reference level.

conditions are essentially related to the local stress state and the in-situ stress field (Moos and Zoback, 1990), which is the foundation to understand the fault mechanism in the vicinity of Nankai subduction zone. In this research, we conducted geomechanical modeling for Site C0002 of the Nankai Trough transect based on riser and riserless drilling to determine the in-situ stress state influence on these drilling parameters. This model explains the borehole observations and drilling problems we faced in previous expeditions. Based on the stress perturbation by regional earthquake events, like occurred off the Kii peninsula in 2004 (Miyake and Koketsu, 2005), an optimally oriented plane (OOP) model of the subduction interface was deployed to estimate the stress field where drilling still does not reach. Comparing the geomechanical model and OOP model helps us to determine the stress state near the Nankai subduction zone.

2. Borehole conditions observation in each drilling stage at Site C0002

The borehole shape and drilling deviation are highly related to in-situ stress observations (Bell and Gough, 1979). For Site C0002, we analyzed the drilling parameters and logging data, including borehole deviation, azimuth, gamma ray, resistivity, rate of penetration (ROP), density, specific gravity (SG), annual mud pressure and velocity (Fig. 2). We have confirmed that the deviations is less than five degrees among these three boreholes, the influence of hole azimuth was negligible in the vertical boreholes (Fig. 2a). Holes C0002A and C0002F cover the depth in between 900 and 1390 mbsf. The gamma ray (Fig. 2b) and resistivity data (Fig. 2c) indicated that even though the measured values in Hole C0002A were jumpy, they fit the trend of those observations in Hole C0002F. That is, the gamma ray increases with depth (89–126 API), and the resistivity kept the range in between 1.9 and 2.8 OHM-m.

Fig. 2d show that the rate of penetration (ROP) was only achieved 15–30 m/h and was as low as 2–15 m/h below 1632 mbsf (Moore et al., 2013) in Hole C0002F, although it was set to be 40 m/h. Hole C0002A and C0002P showed more scattered rate while drilling. Density logging was conducted in Hole C0002A only. To extrapolate the bulk density log to deep portion, the power-law expression has been widely used to estimate the formation density in missing density-log boreholes (Traugott, 1997; Sayers, 2010). We generated a power law equation to fit the density logging curve (Density = $1.168*\mathrm{DEPTH}^{0.073} \pm 0.16$) for estimating the vertical stress (Sv) in the deeper portion of Site C0002 (Fig. 2e). Our calculated Sv at the depth of 875 mbsf was 35.2 MPa, consistence with previous study (Chang and Song, 2016).

The annulus pressure in Hole C0002A is equal to hydrostatic pore pressure. Because the mud weight can be controlled during riser drilling, the APWD in the borehole was maintained between 30 and 45 MPa (Fig. 2f), compared to the hydrostatic pore pressure (29–40 MPa) in Hole C0002F. The higher APWD recorded in Hole C0002P from 54 to 67 MPa.

For the borehole stabilities, a 12 ¼″ × 16 ½″ × 20″ underreamer bottomhole assembly (BHA) was used to drill Hole C0002F at the depth of 875.5–2005.5 mbsf. A 12 ¼″ × 16 ½″ × 20″ underreamer BHA encountered tight conditions while reaming below 1600 mbsf. Below 1600 mbsf, the mud weight in Hole C0002F increased slightly from 1.10 to 1.12 SG reported by Moore et al. (2013). The leak of test (LOT) result (Chang and Song, 2016) showed the formation pressure reached 1.15 SG when the test was performed using 1.10 SG mud. Expedition 348 Scientists and Scientific Participants (2014) reported that Hole C0002P was sidetrack drilled from Hole C0002N to 1936.5 mbsf, and the mud weight increased from 1.16 to 1.32 SG at the bottom of this borehole (Fig. 2g). Stuck pipes were reported in the bottom of this borehole (Expedition 348 Scientists, 2014).

The lithology at that depth is silty claystone interbedded with

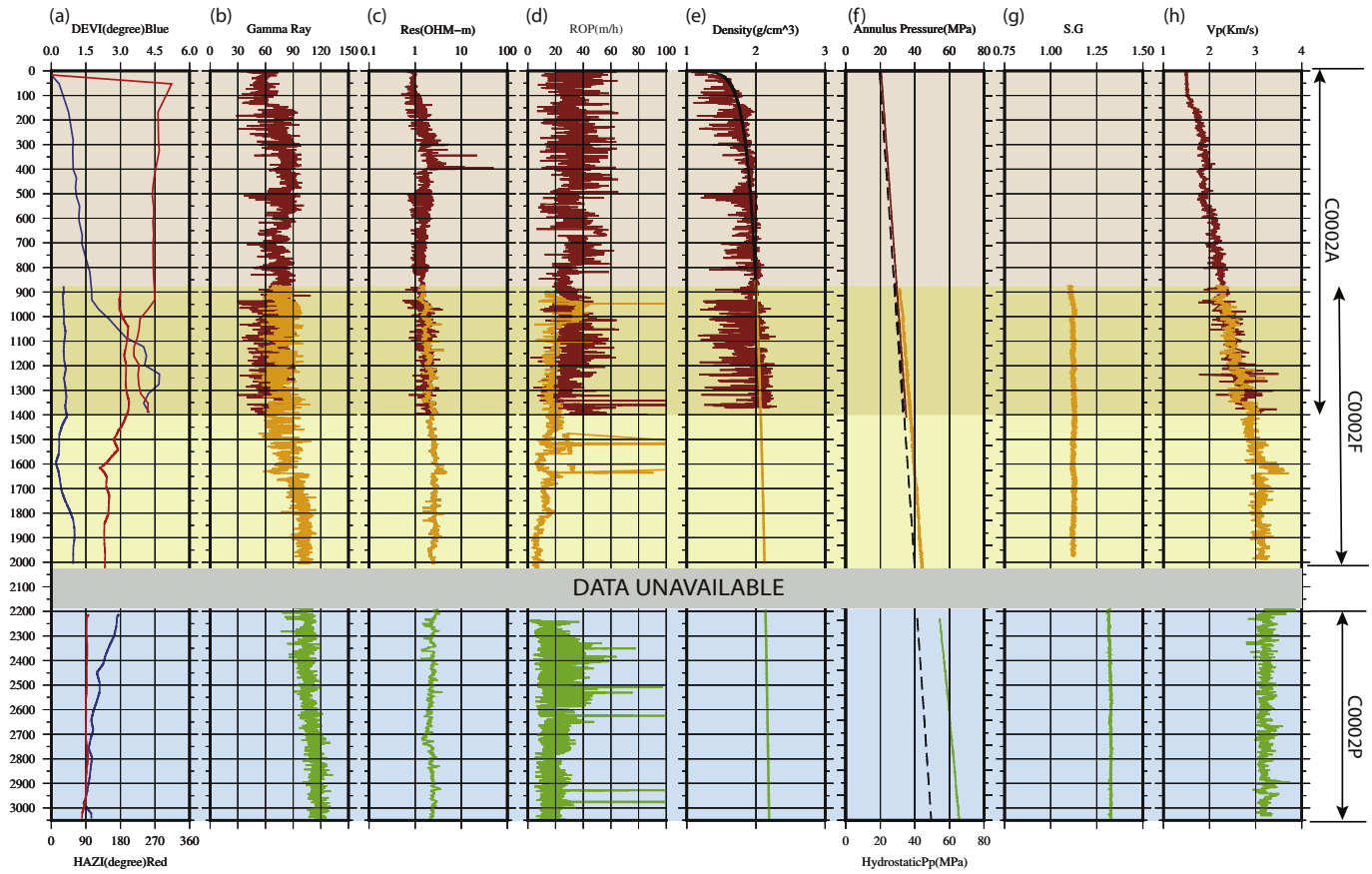

Fig. 2. Borehole conditions and logging data of Hole C0002A C0002F, and C0002P. Including (a) the deviation (in blue line) and borehole azimuth (in red line), (b) gamma ray, (c) resistivity, (d) rate of penetration in meters per hour, (e) density, (f) annulus pressure around borehole wall, (g) specific gravity and (h) P-wave velocity. The overlap section for the quality control starts from 900 to 1390 mbsf. There is a data gap from 2000 to 2200 mbsf.

sandstone recorded in the 348 Expedition preliminary report. All fractures and bedding planes are nearly vertical (dipping angles of 60–90°), the orientation of these existing fractures would not represent the horizontal principal stress orientation. These observations indicate that if the mud weight is close to or occasionally exceeds the tensile fracturing gradient (S_{hmin}), there is potential to reopen existing fractures in previously fractured sediments (rubble zones) by operating the drilling (Jincai and Yin, 2017). The mud circulation in particular would drop/lose in the event of a borehole wall collapse, caving, or massive cutting, which would result in dynamic static losses.

The velocity measurement shows a similar trend as its increasing with depth (1.5–3.2 km/s) in Holes C0002A and C0002F, the consistent P-wave velocity is showing in the overlap section (Fig. 2h). The velocity observed in Hole C0002P shows a minor increase with drilling depth (ca. 3.3 km/s). Comparing the LWD data sets in Site C0002 (Fig. 2), the physical properties like Gamma ray, resistivity, and P-wave velocity are consistent in the overlap section (i.e. at the depth in between 900 and 1390 mbsf). We thus assumed the physical properties and drilling parameters at Site C0002 are laterally homogeneous.

3. Stress states in boreholes C0002A, C0002F, and C0002P

3.1. Method of stress magnitude calculation

Based on the logging data, the physical and drilling trend properties in Holes C0002A and C0002F do not show any significant changes except in mud weight. The horizontal principal stress azimuth in Exp. 314 was determined through borehole breakout and the stress magnitude was estimated by breakout width and rock strength (Chang et al., 2010). However, due to the rare of breakouts in Hole C0002F, it is difficult to determine its horizontal minimum principal stress (S_{hmin}) orientation. Moos and Zoback (1990) proposed a method measured by the borehole annual pressure (Pm) for estimating borehole horizontal principal stresses magnitudes. Based on their study, we estimated the borehole conditions and stress magnitude influenced by the drilling data. We considered an anisotropic stress situation ($S_{HMAX} \neq S_{hmin}$), where S_{HMAX} is the maximum horizontal principal stress, S_{hmin} is the minimum horizontal principal stress, at this site and measured the borehole annual pressure (Pm) to constrain the possible principal stresses. Zoback (2007) suggested that the principal stresses and pore pressure could be used to determine the stress concentration around the borehole. The occurrences of a breakout rely on the rock strength.

Although Chang and Song (2016) mentioned the breakout and tensile observation in Hole C0002F, the number and the quality of the breakouts represent the C ranking judged by World Stress Map criteria (Heidbach et al., 2010). However, the possible breakout or tensile fractures implied that the stress concentration around the borehole wall approaches the rock strength due to the differential stress (S_{HMAX}-S_{hmin}) existed. The concentrated stress closes to the rock strength. Considering the whole sections, few breakouts would not influence the estimation in this study. Based on the LWD image records of “no borehole breakout” and “no tensile fractures” in Holes C0002F and C0002P, we estimated the stress magnitude using the existing borehole breakout in Hole C0002A. Barton et al. (1988) explained how to determine the magnitudes of S_{HMAX} and S_{hmin} at any depth using rock strength and observed breakout width. However, the rock strength estimation is always challenging during scientific drilling. The overlap sections of Holes C0002A and C0002F provide an opportunity to examine the magnitude of principal stresses and rock strength from the depths of 900 to 1390 mbsf. The continuous breakouts were observed in Hole C0002A, which

can infer the magnitudes of its horizontal principal stresses as follows (Zoback et al., 2003).

$$S_{HMAX} = \frac{(C_0 + 2P_p + \Delta P) - S_{hmin}(1 + 2\cos 2\theta_b)}{1 - 2\cos 2\theta_b} \quad (1)$$

where S_{HMAX} is the maximum horizontal principal stress, S_{hmin} is the minimum horizontal principal stress, C_0 is the unconfined compressive strength (UCS), P_p is the hydrostatic pore pressure, ΔP is the differential pressure between the hydrostatic pore pressure and drilling mud pressure and $2\theta_b$ is π minus the breakout width.

Since there is no breakout observed in Hole C0002F, the stress state should be satisfied with the following condition:

$$3S_{HMAX} - S_{hmin} - 2P_p - \Delta P = C_0 \quad (2)$$

At this site, no tensional fracture was discovered. The minimum hoop stress in Holes C0002A and C0002F can be summarized as follows:

$$3S_{hmin} - S_{HMAX} - 2P_p - \Delta P = 0 \quad (3)$$

The hoop stress acting on the borehole wall at the depth 1kmbf (kilometers below sea floor) is clearly shown in Fig. 3. Our assumption is that the stress concentration around the borehole at any given depth is in the critical state, which emphasizes the existence of the differential horizontal stress (i.e. $S_{HMAX} - S_{hmin} > 0$), even when a breakout does not occur on the borehole wall (Wu et al., 2012). The wave crest and trough represent the maximum and minimum values of concentrated stresses in the borehole.

3.2. Stress profiles at Site C0002

For rock strength estimation, we utilized rock strength laboratory experiments from CDEX JAMSTEC and empirical functions used to evaluate the relationship between the rock strength and velocity (Chang et al., 2006), as shown in Fig. 4a. Based on the different breakout behavior in Hole C0002A (60°) and C0002F (0°), the rock strengths (circles in Fig. 4a) in the overlap section can be calculated by the different breakout width. The values of rock strength are higher than those of the experimental results, implying that the rock strength by laboratory experiments in Nankai might be underestimated. Due to saturation of the empirical functions, it is clear showing that the rock strengths growth exponentially when the velocity over 4000 m/s in purple and blue curves (Chang et al., 2006 and Horsrud, 2001, respectively). We used the empirical equation investigated by Lal (1999) (the green line in Fig. 4a) to estimate the rock strength in each section, especially for the deeper portion. Considering the continuous physical properties, our calculation for the borehole stability is based on the PSDM velocity model (Moore et al., 2009) (black line in Fig. 4b), with the MWD velocity data in the boreholes. The maximum velocity will reach approximately 5.2 km/s at the depth of 8 kmbsf as the upper bound rock strength estimation. The sonic logging data indicated that the P-wave velocity at the bottom of Hole C0002P is 3.25 km/s. We extrapolated the velocity logs by power law equation, as the lower bound rock strength. The rock strength profiles from the sea floor to the depth of 8 km, which were calculated from the P-wave velocities, were plotted in Fig. 4c.

According to the Eqs. (1)–(3), the horizontal principal stresses and rock strength can be determined in this overlapping drilling section of

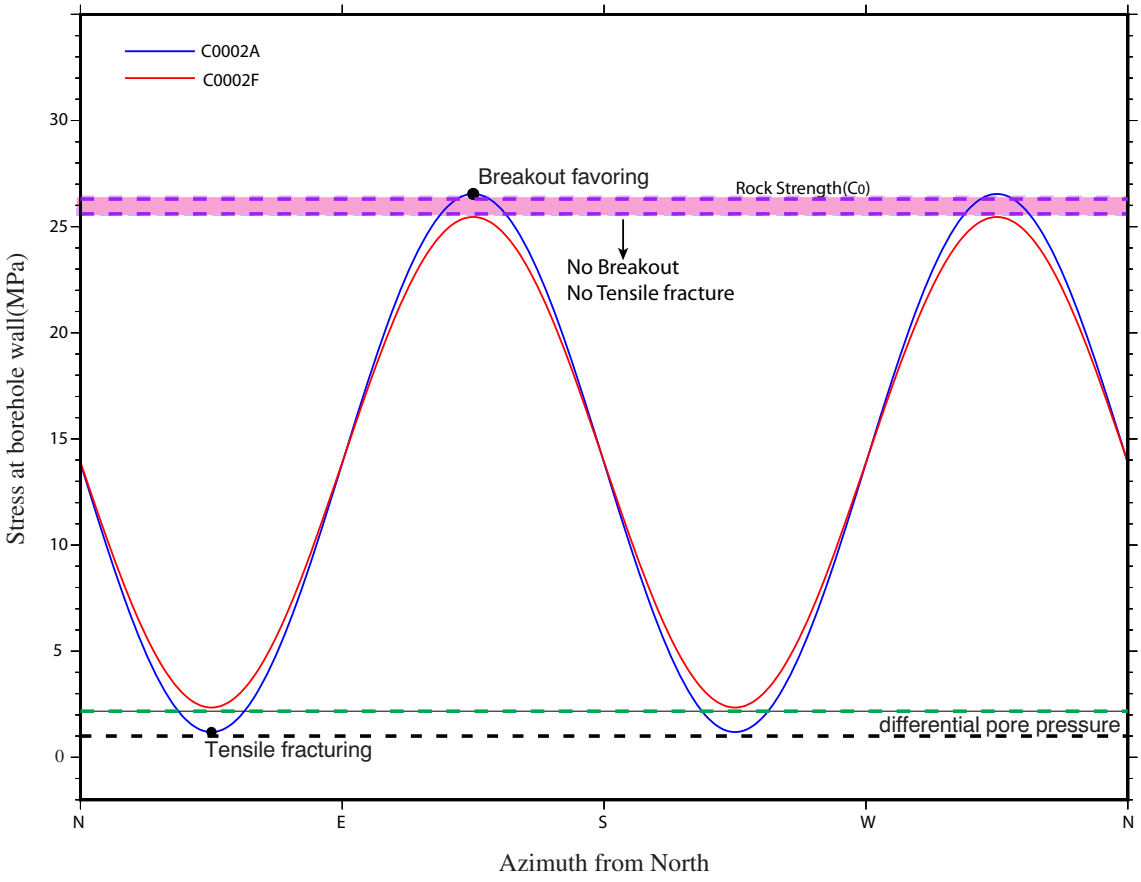

Fig. 3. The concept of the stress concentration in Hole C0002A and Hole C0002F. Blue and red sine curves show the effective stresses bearing on the Hole C0002A and Hole C0002F's borehole wall, respectively. Black and green dash lines show the pore pressure levels in these two boreholes. Note that the breakout was occurred when the effective stress exceeded the rock strength (purple zone between two dash lines).

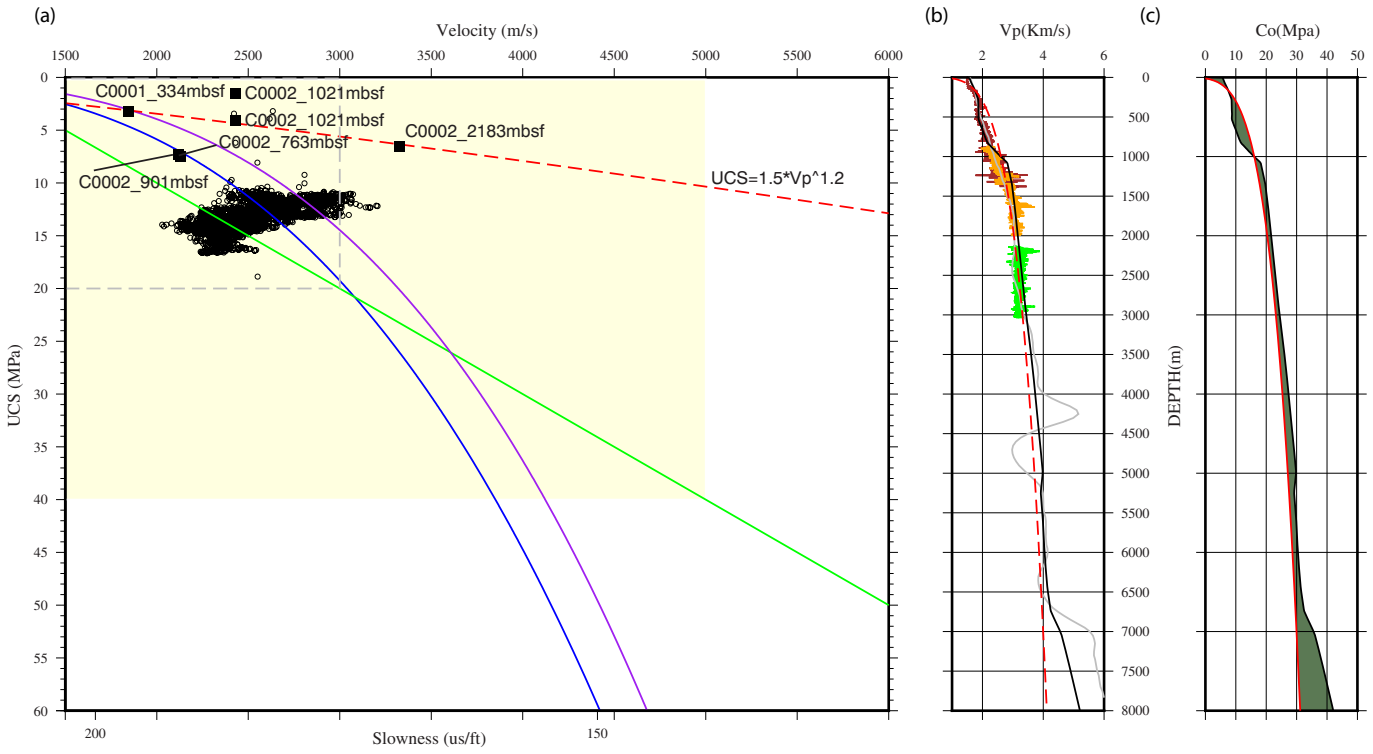

Fig. 4. (a) The estimation plot of rock strength and P-wave velocity, the solid squares represent the USC experiments results measured by CDEX, JAMSTEC. Red dash line is the regression curve of USC experiments. The circles represent the rock strength calculated in repeat sections (900–1390 mbsf) and corresponded to the velocity logging. The purple curve is the empirical function developed in Gulf and Mexico (Chang et al., 2006). The blue curve is the equation developed by Horsrud (2001) in North Sea; the gray dash rectangle marks the maximum rock strength with the velocity in the bottom of Hole C0002P. The empirical relationship developed by Lal (1999) is showing in green curve, the right down edge of the yellow rectangle shows the maximum rock strength represented the corresponding velocity in 5.1 km/s. (b) The velocity profiles used for rock strength estimation, including the logging data (Hole C0002A's Vp plotted in red, Hole C0002F's Vp plotted in orange and Hole C0002P's Vp plotted in green), the velocity models in Moore et al., 2009 (black line) and Kamei et al., 2013 (gray line), the regression equation based on the velocity logs is plotted in red dash line. (c) Rock strength curves converted from empirical function (Lal, 1999) with Moore's velocity model as the upper bound, the lower bound is plotted in red line by the regression equation converted to rock strength, the difference is marked in green.

Holes C0002A and C0002F. The profile of the total effective stresses along the depth from 900 to 1390 mbsf (Fig. 5a) indicates that the maximum horizontal stresses (S_{HMAX}) is lower than the vertical stress (S_v), suggesting a normal faulting stress regime. The similar analysis was reported (Huffman et al., 2016) by assuming low hydrostatic pore pressure in this overlap section without considering the sea water thickness (1939 m). However, the hydrostatic pore pressure in our study is between 29.5 and 34.0 MPa at the depth of 900–1390 mbsf. The consistency of the minimum horizontal principal stress (S_{hmin}) represents the continuous stress profiles with depth at Site C0002 and indicated the less fault zone recorded in the Nankai accretionary wedge. Fig. 5b shows the rock strength and its corresponding P-wave velocity. Notice that the rock strength (10.0–16.6 MPa) is consistent with the velocity measurement range (2–3 km/s). The strength and stress increase at the depth of ca. 1 km reflect the lithology change in the borehole, as we can find the boundary in the seismic profile (Moore et al., 2013) in Fig. 6a.

Considering the abovementioned observations, we constructed a 1-D forward geomechanical model to discuss the stress state at Site C0002. The LWD resistivity images and the drilled boreholes in each stage displaying on the seismic profile (Moore et al., 2013) shows the existing drilling depth (Fig. 6a), which indicate the borehole wall conditions in these 3 boreholes (Holes C0002A, C0002F and C0002P). The horizontal principal stresses to the depth of 3 kmbsf were calculated with the Pm, rock strength and borehole breakout width (0–60°). The LOT results (Moore et al., 2013) between the depth of 900 and 2037 mbsf show a strong agreement with our estimated S_{hmin} magnitude. Clearly, the stress state is subject to the thrust faulting stress regime above the depth of 520 mbsf and then the S_{HMAX} is smaller than the vertical stress at depth, suggesting the normal faulting stress state remains to the bottom of Hole C0002P (at the depth of 3 kmbsf).

Fig. 6c denotes the stress profiles including the depth extend to the depth of 8 kmbsf. We assumed the hydrostatic pore pressure and no breakout occurred below 3 kmbsf. Notice that the high annual pressure (Pm) below 5.5 km depth even exceed to the magnitude of S_{HAMX} if we took the circulated mud weight as 1.35 SG. Our explanation is the stress calculation is constructed on the borehole pressure equilibrium, such overbalanced stress states correspond to the estimation of the lower bound of S_{hmin} and the upper bond of S_{HMAX}. In other words, the stress state in the realistic drilling may higher than our simulation, e.g. harder rock strength, homogeneous horizontal principal stresses (purple area in Fig. 6b). However, for the borehole stability issue and the difficulties occurred in previous drillings, the mud weight setting in Hole C0002P may damage the borehole wall for the deeper drilling at this site. The increasing mud weight over the magnitude of S_{hmin} will lead to wellbore failure and lose mud circulation for deep water drilling, like the case happened in Gulf of Mexico (Lang et al., 2011).

3.3. Borehole stability in drilled boreholes and in the vicinity of subduction zone

In the Expedition 348 preliminary report (Expedition 348 Scientists and Scientific Participants, 2014), the expedition scientists recorded the stuck pipes and borehole wall collapse. Zhang (2013) mentioned that the drilling induced hydraulic fracturing was occurred when the mud pressure was higher than the S_{hmin}. To discuss this borehole stability issue, we constructed a mud pressure model to determine the relationship among the annulus pressure, rock strength, principal stresses

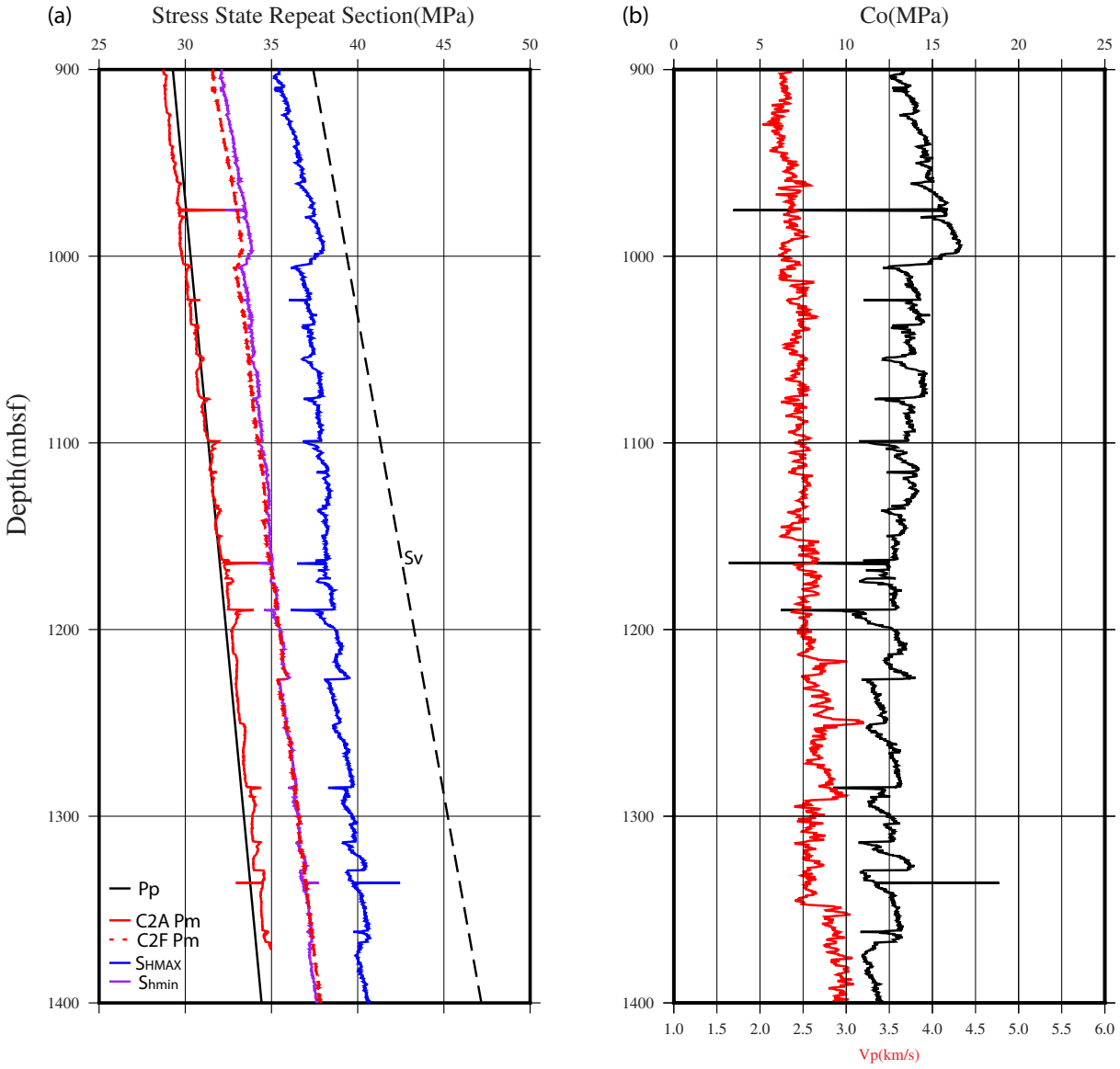

Fig. 5. (a) The stress magnitude plots in the repeat section of Hole C0002A and Hole C0002F. Black dash line shows the magnitude of vertical stress (S_v). Black line is the hydrostatic pore pressure from 900 to 1390 mbsf. The annulus pressure in Hole C0002A is plot in red line. The red dash line is the annulus pressure in Hole C0002F. The horizontal principal stresses, S_{HMAX} and S_{hmin} are plotted in blue line and purple line, respectively. (b) The require rock strength show in black line, the velocity measured from sonic logging represent in red line. The peaks are consistent with the suddenly drop of the annulus pressure.

and borehole breakout width (Moos et al., 2003) (Fig. 7). This stability model showed the optimum mud pressure windows in the possible range between hydrostatic pore pressure and the minimum horizontal principal stresses. At the depth of 500 mbsf (Fig. 7a), the breakout width is a function of the rock strength and mud pressure. Hole C0002A is located in this stability zone and the breakout width was observed by Chang et al. (2010). The breakout width shows that the underbalanced situation in oceanic drilling hardly occurs in the shallow portion. The calculated mud weight window of Hole C0002F (shown in Fig. 7b) at the depth of 1000 mbsf suggests a stability situation with no breakout feature on the borehole wall because the drilling mud pressure is slightly higher the hydrostatic pore pressure. In the middle of Hole C0002P (2500 mbsf), as a result of the high mud weight exceeding the minimum horizontal stress, the tension force rather than the compression pressure affected the borehole wall (Fig. 7c). The rock strength has less influence on the borehole instability in Hole C0002P. Despite the riser drilling providing better control of the mud pressure, the tensile fracturing of the borehole wall occurred within the overpressure state area with low horizontal principal stresses and weak rock strength (such as Hole C0002P). This would explain the occurrence of borehole swelling and pipes becoming stuck.

To estimate the borehole stability in the vicinity of the mega-spray fault, Fig. 7d shows our simulation result at the depth 5 kmbsf in Site C0002 (C0002deep). Our model suggests the optimized mud weight (1.03–1.30 SG) to support the borehole stability for the future deep drilling. In the normal faulting stress state ($Sv > S_{HMAX} > S_{hmin}$), the occurrences of the breakout are an essential index to confirm the borehole stable.

4. Modeled stress state profiles in the Nankai Trough

4.1. Optimally oriented plane modeling

To evaluate the stress status in the Nankai Trough, especially at the depth where the NanTroSEIZE drilling still has not reached the mega-spray fault, we proposed an OOP model based on the concept of the

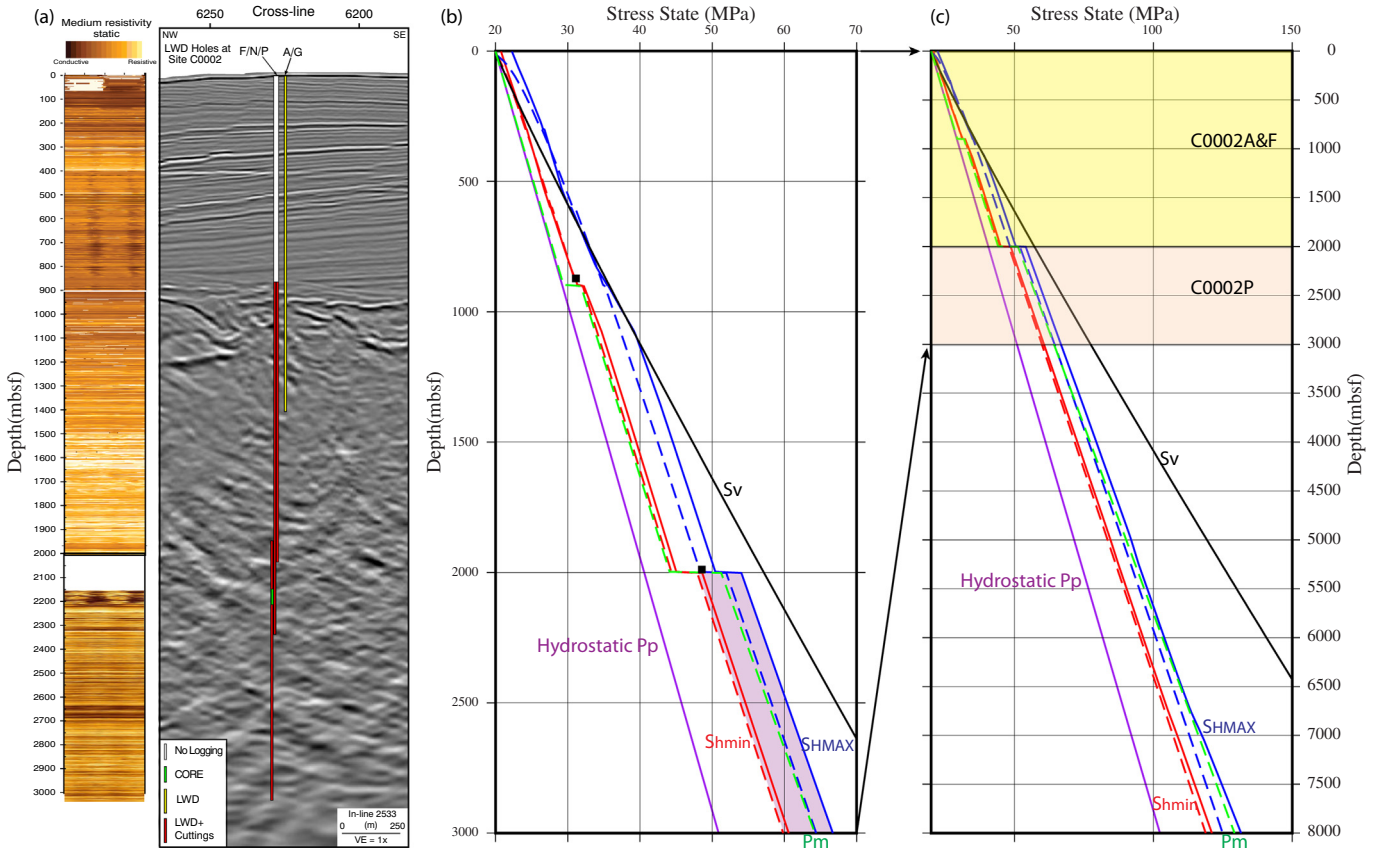

Fig. 6. (a) The LWD resistivity image logs and the drilling stages to different depths with seismic profile. (b) The principal stresses profiles plot to the drilled depth (3 km depth). Black squares are the magnitude of S_{hmin} from LOT tests. The right side is the stress profiles in three principal stresses estimated to the subduction zone, red line and red dash line show the range of S_{hmin} magnitude; blue line and blue dashed line display for the range of S_{HMAX} magnitude, the zone in purple shows the possible range of horizontal principal stresses. The hydrostatic pore pressure plots in purple line, the annulus pressure display in green dash line. The black line show the vertical stress calculated by density log and regression function. (c) The stress profile extend to 8 km depth. Yellow area is the drilling depth of Hole C0002A and Hole C0002F; orange area is the drilling section of Hole C0002P.

Coulomb failure stress (CFS) (Harris, 1998; Cocco and Rice, 2002; and references therein), which can be expressed as follows:

$$CFS = \tau + \mu'\sigma_n, \tag{4}$$

where τ is the shear stress computed along the slip direction on the assumed plane; μ' is the apparent friction coefficient, defined as $\mu' = \mu(1 - B)$, where B is the Skempton's coefficient, and is the normal stress to the assumed plane. Previous studies (e.g., Cocco and Rice, 2002; Chan and Stein, 2009) found insignificant differences in the results of Coulomb stress given the inevitable uncertainties in apparent friction coefficient (in between 0.2 and 0.8) and Skempton's coefficient (in between 0.5 and 0.9). In this study, thus, we only represented the results for an intermediate value of 0.4 for apparent friction coefficient.

Calculating the *CFS* requires a receiver fault plane, assumed to be the OOP. An OOP is determined using the summarized Coulomb failure stress contributed from all possible stress sources (King et al., 1994). In terms of the stress regime, τ and σ_n can also be expressed as follows:

$$\tau = \frac{1}{2}(\sigma_1 - \sigma_3)\sin 2\beta \tag{5}$$

$$\sigma_n = \frac{1}{2}(\sigma_1 + \sigma_3) - \frac{1}{2}(\sigma_1 - \sigma_3)\cos 2\beta, \tag{6}$$

where β is the orientation from the σ_1 axis to the assumed plane. The polarities of σ_1 and σ_3 are perpendicular to each other. Then, the *CFS* formula, which was originally represented in Eq. (4), becomes the following:

$$CFS = \frac{1}{2}(\sigma_1 - \sigma_3)(\sin 2\beta - \mu'\cos 2\beta) - \frac{1}{2}\mu'(\sigma_1 + \sigma_3). \tag{7}$$

Differentiating Eq. (7) as a function of β and making this equation zero allows us to find the plane orientation at which the Coulomb failure stress is at its maximum, which is meaning we can constrain the 3 principal stress azimuths. In the other word, the faulting stress regime (Normal, Strike-Slip, and Thrust) can be illustrated by this model. This plane is set to OOP, which satisfies the following equation:

$$\tan 2\beta = -1/\mu'. \tag{8}$$

We computed the OOP using the COULOMB 3.4 code developed by Toda and Stein (2002).

4.2. Modeled stress states at Site C0002

To properly model the OOP for Site C0002, we considered several sources that impacted the stress field, including the slip deficit along the Nankai megathrust, the coseismic dislocations of the two September 5th, 2004 earthquakes with M 7.2 and 7.3, respectively, and the April 1st, 2016 earthquake with M 6.0 (black stars in Fig. 1b). The stress orientation at shallow (the depth of 1 kmbsf) is observed Wu et al. (2013) to examine the lateral stress filed change of our OOP models. To confirm the stress status in the vicinity of a subduction system (the depth of 5 kmbsf), we determined the OOP to constrain the faulting mechanics in the Nankai Trough.

The rupture potential of a fault system can be modeled using a slip deficit model (Segall and Harris, 1986). After the occurrence of a

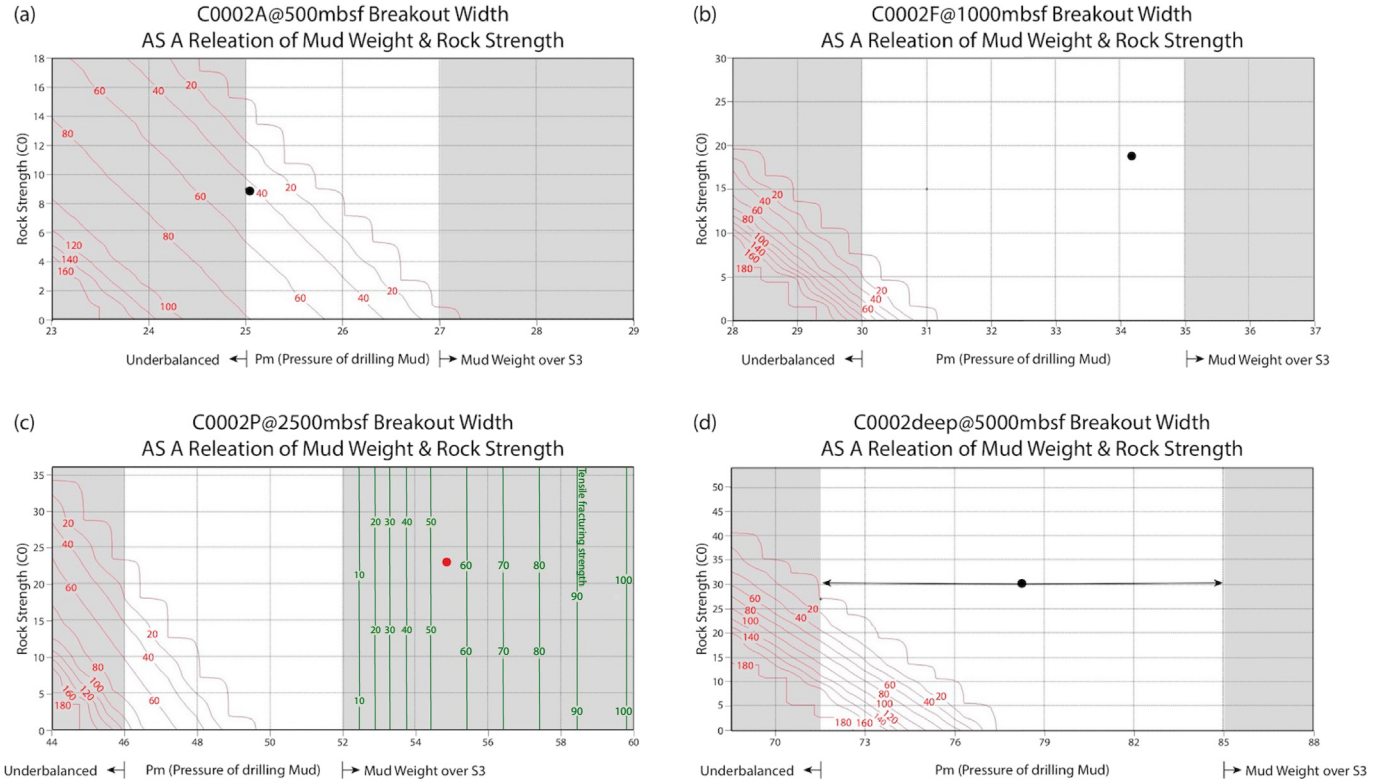

Fig. 7. Borehole stability model in each represented depth. (a) Mud windows in 500mbsf (Hole C0002A), black cycles show the stress state in corresponding rock strength and breakout width in our model. Gray zones indicated the underbalanced state and the annual pressure over the S_{hmin}. Red contours show the possible width of breakout. (b) Mud window in 1000 mbsf (Hole C0002F), the stress state and annual pressure in the stabile zone and no breakout occurred. (c) Mud windows in 2500 mbsf (Hole C0002P), red dot indicated the critical status that borehole in the unstable situation. The tensile fracturing strength (green line) indicates the rubble zone created by tension force. (d) Mud windows in 5000 mbsf near the mega-spray fault (Site C0002deep), keep low annual pressure in this section helping us to observe the forming of breakout and monitoring the borehole stabilities.

characteristic earthquake, the slip deficit on a fault system has been compensated (i.e. accumulated stress has been totally released) and the stress regime in the vicinity has been reset and is close to isotropy (Chan et al., 2012). During an interseismic period, the slip potential (known as coupling) of a fault system accumulates and can be modeled using a slip deficit model (Segall and Harris, 1986). For the Nankai Trough megathrust system, Yokota et al. (2016) obtained a slip deficit model using both the seafloor geodetic observation network developed by the Hydrographic and Oceanographic Department of the Japan Coast Guard (AsADA and Yabuki, 2001) and Japanese GPS Earth Observation Network (GEONET) data. Due to better constraints through near-field observations, our model would be reliable for illustrating the slip deficit behavior near Site C0002. We assumed the stress along the Nankai megathrust was completely released after the M 8.2 1944 Tonankai and the M 8.3 1946 Nankaido earthquakes (Liu et al., 2010). Therefore, a 60-year period is considered in the slip deficit model.

In 2004, two M ≥ 7.0 earthquakes took place near the surface trace of the Nankai Trench. In addition, an M 6.0 earthquake took place near Site C0002, which could also perturb the stress state (Wu et al., 2013). Calculating OOP requires some earthquake rupture parameters, including rupturing fault dimension and slip magnitude. Since no detailed rupture model is available for these three events, alternatively, spatial-homogenous slip models were adopted. We implemented the source parameters of the two 2004 and 2016 earthquakes obtained from Bai et al. (2007) and the Global Centroid-Moment-Tensor (CMT, http://www.globalcmt.org), respectively. We then determined rupture dimensions and average slips according to the scaling law of Wells and Coppersmith (1994) and corresponding magnitudes, and assumed their hypocenters as the centers of earthquake ruptures.

By implementing the slip deficit of the Nankai Trough and slip dislocations of the three earthquakes, we evaluated the OOPs at various depths at Site C0002 (Fig. 8). Due to the unclear structural geometry, we proposed three stress orientation models, considering different locations of the megathrust and splay fault. We demonstrated three cases of modeled stress orientations with depth, considering different locations of the megathrust and splay fault (Fig. 8). All results indicate that the stress mechanics remain in the normal faulting stress regime (i.e., dip angles of σ_1 are > 45°) above the megathrust, corresponding to the LOT results. The existence of the splay fault results in a stress disturbance on the hanging wall (Fig. 8c), whereas the main principal stress is subjected to overburden weight (vertical stress) at the drilling site. Notice that the minimum principal stress (σ_3) is rotated to the vertical axis below the depth of the subduction zone. This simulation indicates that the stress state is converted to a thrust faulting stress regime ($S_{HMAX} > S_{hmin} > S_v$) below the megathrust rupture zone.

5. Conclusions

Based on our analysis, we determined the stress state and rock strength in the overlap sections of Hole C0002A and Hole C0002F and built a geomechanical model to constrain the stress magnitude in Hole C0002P. A high mud weight applied to the borehole make the borehole annulus pressure exceed the magnitude of S_{hmin} in the borehole and diminish the borehole breakout occurrence in Hole C0002P. Swelling occurred anywhere due to the enlargement of the borehole. The growing, nondirectional tensile failures around the borehole wall increase the volume of cuttings and the drilling pipes became stuck at the end of the casing, even at the bottom of the borehole. The low horizontal principal stresses (S_{HMAX} and S_{hmin}) explain the difficulties in the Hole C0002P drilling.

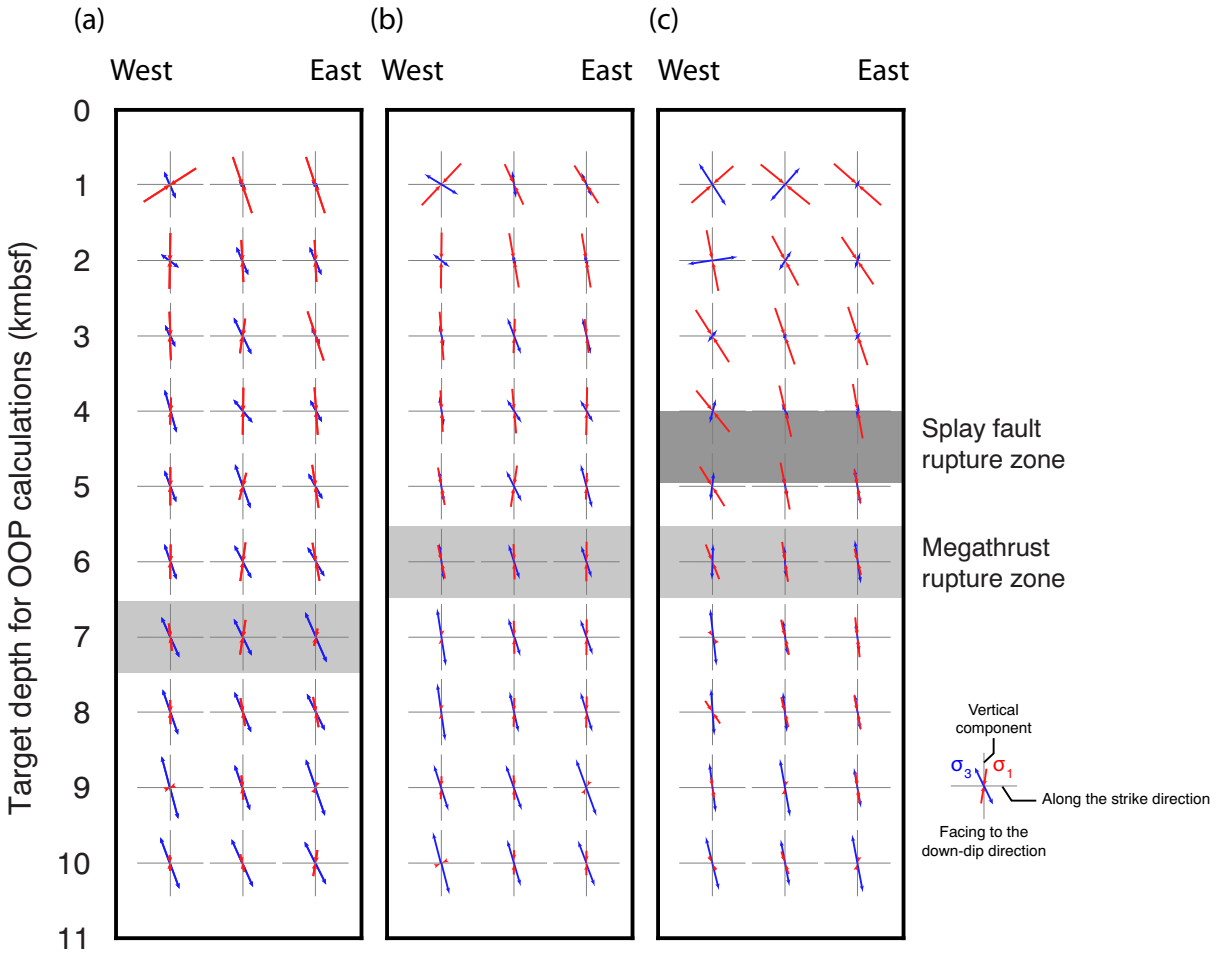

Fig. 8. To properly model OOP for Site C0002, we considered the 60-year slip deficit along the Nankai megathrust proposed by Yokota et al. (2016), the coseismic dislocations of two 2004 earthquakes and one 2016 earthquake. Three cases of the modeled OOP along the depth on Site C0002, showing stress regimes when (a) the megathrust cuts at the depth of 7 kmbsf; (b) the megathrust cuts at the depth of 6 kmbsf; and (c) a splay fault cuts at the depth of 4.5 kmbsf and the megathrust cuts at the depth of 6 kmbsf. Red and blue arrows represent orientations of the maximum (σ_1) and minimum (σ_3) stress axes, respectively, on lateral projection plane, i.e., when σ_1 plunge $<$ 45° and σ_3 plunge $>$ 45° suggests OOP favorable to thrust faulting; σ_1 plunge $>$ 45° and σ_3 plunge $<$ 45° suggests OOP favorable to normal faulting; both σ_1 and σ_3 plunges $<$ 45° suggests that OOP favorable to strike-slip faulting. Black and gray zones represent assumed locations of the megathrust and a splay fault, respectively.

Through a stress state estimation and by observing logging data, OOP model predicted the stress state in the vicinity of the Nankai subduction zone, where is hard to reach. The normal faulting stress regime OOP model simulated at this site indicates a low magnitude of S_{hmin} and consistent with the stress profile we estimated in the geomechanical model. Respecting to maintain the balance state in the borehole, the optimized mud weight applied in the borehole should be less than S_{hmin}. The overestimated mud weight might induce the number of borehole breakouts and tensile fractures, especially in the low horizontal principal stresses area.

The geomechanical model can be implemented to estimate the stress magnitude based on the drilling process, and this model is necessary to maintain the drilling in the stability stage. On the other hand, it may be risky to drill the borehole without the information from real-time logging information. The OOP models combined the geomechanical model provide the method to evaluate the stress magnitude and stress regime based on the observation data and slip-deficit in the Nankai Trough area. These results show the low horizontal principal stresses in the normal faulting stress regime above the mega-spray fault and imply that the locked zone of the Nankai Trough. The stress anomaly (orientation and magnitude) may occur below the Nankai subduction zone.

Acknowledgement

We thank CDEX, JAMSTEC for providing logging data and technical support. We are also grateful for kind support from the International Ocean Discovery Program and Expedition 314, 338, and 348 onboard scientists. Data used for this article were obtained from the SIO7 Data Center at JAMSTEC. The datasets supporting the conclusions of this article is available in the database of IODP expedition of D/V Chikyu, http://sio7.jamstec.go.jp/well-logging/. This research is partially supported by the National Research Foundation Singapore and the Singapore Ministry of Education under the Research Centres of Excellence initiative.

References

AsADA, A., Yabuki, T., 2001. Centimeter-level positioning on the seafloor. Proc. Jpn. Acad. Ser. B 77 (1), 7–12.

Bai, L., Bergman, E.A., Engdahl, E.R., Kawasaki, I., 2007. The 2004 earthquakes offshore of the Kii peninsula, Japan: hypocentral relocation, source process and tectonic implication. Phys. Earth Planet. Inter. 165 (1–2), 47–55. https://doi.org/10.1016/j.pepi.2007.07.007.

Barton, C.A., Zoback, M.D., Burns, K.L., 1988. In-situ stress orientation and magnitude at the Fenton geothermal site, New Mexico, determined from wellbore breakouts. Geophys. Res. Lett. 15. https://doi.org/10.1029/88GL02106.issn: 0094-8276.

Bell, J.S., Gough, D.I., 1979. Northeast-southwest compressive stress in Alberta: evidence

from oil wells. Earth Planet. Sci. Lett. 45, 475–482.
Chan, C.H., Stein, R.S., 2009. Stress evolution following the 1999 Chi-Chi, Taiwan, earthquake: consequences for afterslip, relaxation, aftershocks and departures from Omori decay. Geophys. J. Int. 177 (1), 179–192.
Chan, C.H., Hsu, Y.J., Wu, Y.M., 2012. Possible stress states adjacent to the rupture zone of the 1999 Chi-Chi, Taiwan, earthquake. Tectonophy 541–543, 81–88. https://doi.org/10.1016/j.tecto.2012.03.031.
Chang, C., Zoback, M., Khaksar, A., 2006. Empirical relations between rock strength and physical properties in sedimentary rocks. J. Pet. Sci. Eng. 51, 223–237.
Chang, C., McNeill, L.C., Moore, J.C., Lin, W., Conin, M., Yamada, Y., 2010. In situ stress state in the Nankai accretionary wedge estimated from borehole wall failures. Geochem. Geophys. Geosyst. 11, Q0AD04. https://doi.org/10.1029/2010GC003261.
Chang, C., Song, I., 2016. Present-day stress states underneath the Kumano basin to 2 km below seafloor based on borehole wall failures at IODP site C0002, Nankai accretionary wedge. Geochem. Geophys. Geosyst. 17 (11), 4289–4307. https://doi.org/10.1002/2016gc006562.
Cocco, M., Rice, J., 2002. Pore pressure and poroelasticity effects in Coulomb stress analysis of earthquake interactions. J. Geophys. Res. 107 (0). https://doi.org/10.1029/2000JB000138.
Expedition 348 Scientists and Scientific Participants, 2014. NanTroSEIZE Stage 3: NanTroSEIZE plate boundary deep riser 3. In: IODP Prel. Rept, pp. 348. https://doi.org/10.2204/iodp.pr.348.2014.
Wells, Donald, Coppersmith, K., 1994. New empirical relationships among magnitude, rupture length, rupture width, rupture area, and surface displacement. Bull. Seismol. Soc. Am. 84, 974–1002.
Harris, R.A., 1998. Introduction to special section: stress triggers, stress shadows, and implications for seismic hazard. J. Geophys. Res. 103, 24,347–324,358.
Heidbach, O., Tingay, M., Barth, A., Reinecker, J., Kurfeß, D., Müller, B., 2010. Global crustal stress pattern based on the World Stress Map database release 2008. Tectonophysics 482 (1–4), 3–15. https://doi.org/10.1016/j.tecto.2009.07.023.
Horsrud, P., 2001. Estimating mechanical properties of shale from empirical correlations. SPE Drill. Complet. 16 (2), 68–73.
Huffman, K.A., Saffer, D.M., Dugan, B., 2016. In situ stress magnitude and rock strength in the Nankai accretionary complex: a novel approach using paired constraints from downhole data in two wells. Earth Planets Space 68, 123.
Jincai, Zang, Yin, Shang-Xian, 2017. Fracture gradient predication: an overview and an improved method. Pet. Sci. 14 (4), 720–730.
Kamei, R., Pratt, R.G., Tsuji, T., 2013. On acoustic waveform tomography of wide-angle OBS data – strategies for pre-conditioning and inversion. Geophys. J. Int. 194, 1250–1280. https://doi.org/10.1190/1.2904554.
Kinoshita, M., Tobin, H., Moe, K.T., the Expedition 314 Scientists, 2008. NanTroSEIZE Stage 1A: NanTroSEIZE LWD transect. IODP Prel. Rept. 314. https://doi.org/10.2204/iodp.pr.314.2008.
King, G.C.P., Stein, R.S., Lin, J., 1994. Static stress changes and the triggering of earthquakes. Bull. Seismol. Soc. Am. 84, 935–953.
Lal, M., 1999. Shale stability: drilling fluid interaction and shale strength, SPE 54356. In: SPE Latin American and Carribean Petroleum Engineering Conference. Society of Petroleum Engineering, Caracas, Venezuela.
Lang, James, Li, Shuling, Zhang, Jon, 2011. Wellbore Stability Modeling and Real-time Surveillance for Deepwater Drilling to Weak Bedding Planes and Depleted Reservoirs. SPE/IADC 139708. https://doi.org/10.2118/139708-MS.
Liu, Zhen, Owen, Susan, Dong, Danan, Lundgren, Paul, Webb, Frank, Hetland, E., Simons, Mark, 2010. Estimation of interplate coupling in the Nankai Trough, Japan using GPS data from 1996 to 2006. Geophys. J. Int. 181. https://doi.org/10.1111/j.1365-246X.2010.04600.x.
Miyake, H., Koketsu, K., 2005. Long-period ground motions from a large offshore earthquake: the case of the 2004 off the Kii peninsula earthquake, Japan. Earth Planets Space 57, 203. https://doi.org/10.1186/BF03351816.
Moore, G.F., Park, J.-O., Bangs, N.L., Gulick, S.P., Tobin, H.J., Nakamura, Y., Sato, S., Tsuji, T., Yoro, T., Tanaka, H., Uraki, S., Kido, Y., Sanada, Y., Kuramoto, S., Taira, A., 2009. Structural and seismic stratigraphic framework of the NanTroSEIZE Stage 1 transect. In: Proceedings of the Integrated Ocean Drilling Program. vol. 314/315/316 Integrated Ocean Drilling Program Management International, Inc., Washington, DC. https://doi.org/10.2204/iodp.proc.314315316.102.
Moore, G., Kanagawa, K., Strasser, M., Dugan, B., Maeda, L., Toczko, S., the Expedition 338 Scientists, 2013. NanTroSEIZE Stage 3: NanTroSEIZE plate boundary deep riser 2. In: IODP Prel. Rept, pp. 338. https://doi.org/10.2204/iodp.pr.338.
Moos, D., Zoback, M.D., 1990. Utilization of observations of well bore failure to constrain the orientation and magnitude of crustal stresses: application to continental deep Sea drilling project and ocean drilling program boreholes. J. Geophys. Res. 95, 9305–9325.
Moos, D., Peska, P., et al., 2003. Comprehensive wellbore stability analysis using quantitative risk assessment. J. Pet. Sci. Eng. 38, 97–109 Spec. Issue on Wellbore Stability. B. S. Aadnoy and S. Ong.
Sayers, C., 2010. Geophysics under stress: geomechanical applications of seismic and borehole acoustic waves. In: SEG Distinguished Instructor Short Course, Distinguished Instructor Series No. 13, https://doi.org/10.1190/1.9781560802129.
Segall, P., Harris, R., 1986. Slip defttit on the Parkfield, California section of the San Andreas fault as revealed by inversion of geodetic data. Science 233, 1404–1413.
Seno, T., Stein, S., Gripp, A.E., 1993. A model for the motion of the Philippine Sea plate consistent with NUVEL-1 and geological data. J. Geophys. Res. 98. https://doi.org/10.1029/93JB00782.
Toda, S., Stein, R.S., 2002. Response of the San Andreas Fault to the 1983 Coalinga-Nuñez Earthquakes: an application of interaction-based probabilities for Parkfield. J. Geophys. Res. 107. https://doi.org/10.1029/2001JB000172.
Traugott, M., 1997. Pore pressure and fracture pressure determinations in deepwater. In: World Oil: Deepwater Technology Special Supplement. vol. 218. pp. 68–70. http://www.hxrdrillingservices.com/wp-content/uploads/WorldOil.pdf.
Wu, Hung-Yu, Kinoshita, Masataka, Sanada, Yoshinori, 2012. Stress state estimation by geophysical logs in NanTroSEIZE Expedition 319-Site C0009, Kumano Basin, southwest Japan. Geophys. Res. Lett. 39. https://doi.org/10.1029/2012GL053086.
Wu, Hung-Yu, Chan, C–.H., Kinoshita, M., Saito, S., 2013. Stress field observation and modeling from the NanTroSEIZE scientific drillings in the Nankai Trough system, SW Japan. Tectonophysics 600, 99–107.
Yokota, Y., Ishikawa, T., Watanabe, S.I., Tashiro, T., Asada, A., 2016. Seafloor geodetic constraints on interplate coupling of the Nankai Trough megathrust zone. Nature 534 (7607), 374.
Zhang, J., 2013. Borehole stability analysis accounting for anisotropies in drilling to weak bedding planes. Int. J. Rock Mech. Min. Sci. 60, 160–170.
Zoback, M., 2007. Reservoir Geomechanics. Combridge University Press, New York.
Zoback, M.D., Barton, C.A., Brudy, M.O., Castillo, D.A., Grollimund, B.R., Finkbeiner, T., Moos, D.B., Peska, P., Ward, C.D., Wiprut, D.J., 2003. Determination of stress orientation and magnitude in deep wells, 2003. Int. J. Rock Mech. Min. Sci. 40, 1049–1076.